Journal of Inorganic and General Chemistry
ZAAC
Zeitschrift für anorganische und allgemeine Chemie
www.zaac.wiley-vch.de
RESEARCH ARTICLE
DOI: 10.1002/zaac.202200168

$Ca_{14}FeAs_{11}$ – A structure comprising structural motifs of iron-based superconductors and Ca-As Zintl phases

Andrea V. Hoffmann,[a] Thomas F. Fässler,*[a] and Viktor Hluhyy*[a]

Dedicated to Prof. Thomas Schleid on the Occasion of His 65th Birthday

$Ca_{14}FeAs_{11}$ is the first iron-containing representative of the $Ca_{14}AlSb_{11}$ structure type and the first compound with isolated $FeAs_4$ tetrahedra. It can be regarded as a salt-like compound containing isolated $[FeAs_4]^{9-}$ tetrahedra, linear $[As_3]^{7-}$ units, isolated As^{3-} anions and Ca^{2+} cations and thus is a borderline compound between binary Fe–As intermetallics and salt-like calcium arsenides. $Ca_{14}FeAs_{11}$ is obtained by a two-step high-temperature reaction, in which preformed FeAs alloy is heated with Ca in the presence of additional As in a sealed silica tube. Structure determination from single crystals at 150 K reveal the $Ca_{14}AlSb_{11}$ structure type with space group $I4_1/acd$ ($Z=8$, $a=15.6268(2)$ Å, $c=20.9781(5)$ Å, and $V=5122.79(15)$ Å^3). Band structure calculations predict metallic properties with strong contribution of Fe orbitals to the density of states at the Fermi level.

Introduction

The definition of Zintl phases is generally restricted to intermetallic compounds that are built up by two or more main group (semi)metal components. However, if the transition metal forms covalent bonds to main-group atoms or if an oxidation states can unequivocally be assigned to the transition metal, the term Zintl phase can be extended. In this context replacement of main group metal atoms by a transition metal atoms in isotypic structures can give a deeper insight as the multitude of compounds with metals in the ratio 14:1:11 does.

The $Ca_{14}AlSb_{11}$ structure type was first mentioned by *Schäfer et al.* in 1984,[1] and a large number of new compounds $A_{14}TPn_{11}$ (A = alkaline earth-, rare earth-metals, T = Mg, group 13 or transition metal elements, Pn = pnictide elements) has been synthesized and investigated in the last two decades.[2–14,15] The subsequent interest in these structurally complex phases has arised from their interesting electronic and magnetic properties that depend on the composition. The group of *Kauzlarich* is engaged in the study of this family of compounds as promising thermoelectric materials.[10] The compounds either display ferromagnetic or antiferromagnetic behavior (T = Mn, Pn = Sb, Bi)[3,4,9,13,16] or paramagnetic behavior following Curie-Weiss law (T = Mn, Pn = As,P)[4,7,15] at lower temperatures and are narrow-gap semiconductors (T = Al, Ga; Pn = Sb, As).[2,4,5] $Eu_{14}MnSb_{11}$ has the highest ferromagnetic-paramagnetic phase transition temperature within this class of compounds ($T_C=92$ K).[17] The analogous indium-containing species are mostly Curie-Weiss paramagnets except for $Eu_{14}InSb_{11}$.[16] $Yb_{14}MnSb_{11}$ and $Yb_{14}ZnSb_{11}$ both show weak metallic behavior, and the Zn compound contains intrinsic Yb^{2+} and Yb^{3+} states.[12] For $Eu_{14}MnSb_{11}$ a giant magnetoresistance (GMR, sometimes also called colossal magnetoresistance, CMR) has been reported.[17] $Yb_{14}MnSb_{11}$ has moved into focus since it turned out to be a better thermoelectric material than p-$Si_{1-x}Ge_x$.[18]

The structure of these compounds can be described in terms of a Zintl phase containing a $[TPn_4]^{9-}$ tetrahedron, a linear $[Pn_3]^{7-}$ unit, four isolated Pn^{3-} anions, and fourteen interstitial A^{2+} cations per formula unit. For the first compound of this family, $Ca_{14}AlSb_{11}$, no positional disorder within the linear $[Sb_3]^{7-}$ unit were reported. In case of the isostructural compounds $A_{14}AlSb_{11}$ with A = Sr and Ba, an increasing disorder for the central atom of the $[Sb_3]^{7-}$ unit was detected,[2] and the same positional disorder within the Pn_3 unit was observed in the compounds containing P and As .[4–7,19] The disorder of the central atom of the trimeric unit is stronger for the P compounds, so that the $[Pn_3]^{7-}$ unit can alternatively be described as a $[Pn_2]^{4-}$ dumbbell linearly coordinated to an isolated Pn^{3-} atom.[6,7,15,19] In the corresponding As compounds this disorder is less pronounced.[4,5] The isolated $[TPn_4]^{9-}$ tetrahedra are distorted in all compounds and flattened in the *ab* plane. The strongest distortion is observed for the Mn compounds and is earlier attributed to a d^4 *Jahn-Teller* distortion.[4,8] In most of $A_{14}TPn_{11}$ compounds the metal T has according to the Zintl-Klemm concept the oxidation state 3+, which has been confirmed by magnetic

[a] A. V. Hoffmann, Prof. T. F. Fässler, Dr. V. Hluhyy
Department of Chemistry,
Chair of Inorganic Chemistry with Focus on Novel Materials,
Technical University of Munich, < street/
Lichtenbergstr. 4, D-85747
Garching, Germany
E-mail: thomas.faessler@lrz.tum.de
viktor.hluhyy@lrz.tum.de

Supporting information for this article is available on the WWW under https://doi.org/10.1002/zaac.202200168

measurements.[2,4–6,15,16,19] However, there are representatives of the same structural type with $T=Mg^{2+}$, Mn^{2+}, Zn^{2+} and Cd^{2+}, which cannot all be considered as classical Zintl phases.[20,21] Kauzlarich *et al.* have shown e.g. that $Ca_{14}MnP_{11}$ displays a paramagnetic moment most consistent with an oxidation state of +2 for Mn, and in this case the tetrahedra are less distorted.[7]

Concerning chemical bonding, the transition metal-containing compounds with the structure type $Ca_{14}AlSb_{11}$ represent an interesting transition from typical intermetallic compounds to electron-precise, semiconducting Zintl phases, since, as outlined below, these compounds comprise at the same time structural units of the related binary intermetallic compounds with TPn_4 tetrahedra and polyanions with *Pn-Pn* bonds.

As can be seen in Figure 1, the ternary phase system Ca–Fe-As so far contains three ternary compounds: $CaFe_2As_2$,[22] $CaFe_4As_3$ [23] and $CaFe_5As_3$.[24] They share the structural motif of $FeAs_4$ tetrahedra, which are connected differently. Above 170 K the Ca-richest species $CaFe_2As_2$ crystallizes in the $ThCr_2Si_2$ structure type (space group *I*4/*mmm*) and below 170 K in the $SrFe_2As_2$ structure type (space group *Fmmm*). It contains layers of edge-sharing $FeAs_4$ tetrahedra.[25] At higher pressures these layers, which are separated by Ca atoms, approach each other under formation of As–As bonds between As atoms of different layers, leading to a three-dimensional (3D) $FeAs_4$ network.[22] As a consequence, the oxidation state of Fe changes from +3 at ambient pressure to +2 at higher pressure in the so-called "collapsed" structure. In $CaFe_4As_3$[23] the layers of the $FeAs_4$ tetrahedra are interconnected by corner sharing and under formation of connected, Fe-centered As_5 pyramids with the Ca atoms located in the channels that occur along the *b* direction. The Fe-richest ternary compound, $CaFe_5As_3$,[24] shows the same structure motifs as $CaFe_4As_3$, but the layers are packed closer with tetrahedra sharing As atoms between the layers and less Ca atoms located in the channels.

We now report another ternary compound $Ca_{14}FeAs_{11}$, which comprises both structural motifs, namely $FeAs_4$ tetrahedra and polyarsenide anions and thus can be regarded as a borderline compound between the binary Fe–As intermetallics and salt-like calcium arsenides.

Experimental Section

Synthesis. The title compound $Ca_{14}FeAs_{11}$ has been synthesized via solid-state reaction. Sample preparation and manipulations were done under protective atmosphere in an argon-filled glove box (MBraun 20G, argon purity 99.998%). Starting materials were elements of high purity: ingots of calcium (Alfa Aesar, 99.5%), iron powder (ChemPur, 99.9%) and arsenic pieces (ChemPur, 99.999%). For the ternary compound a two-step synthesis was performed. First, a mixture of Fe and As (1:1 stoichiometry) was transferred into a niobium ampoule which was sealed and then placed in a silica tube. The mixture was heated to 973 K for 40 h. The precursor

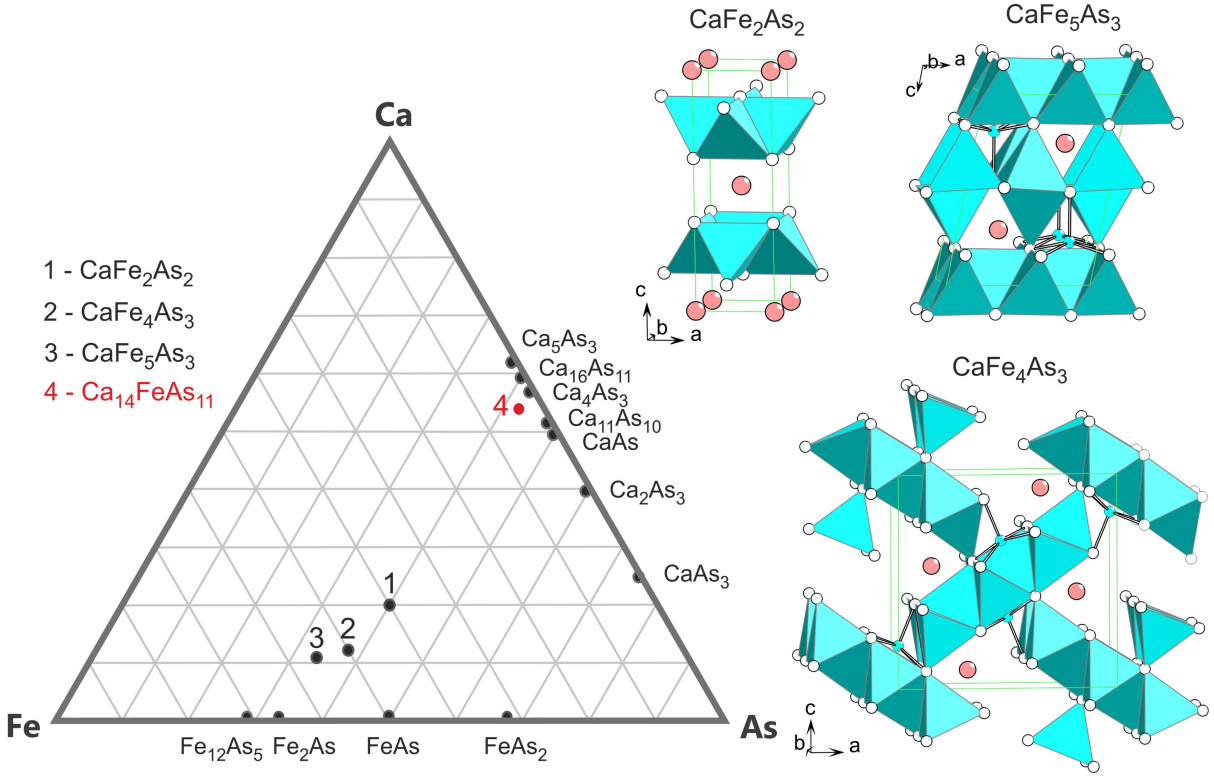

Figure 1. The ternary Ca–Fe–As composition diagram (left). The known phases **1** to **3** and novel $Ca_{14}FeAs_{11}$ (**4**) are marked with filled black and red circles, respectively. The crystal structures of $CaFe_2As_2$ (**1**), $CaFe_4As_3$ (**2**) and $CaFe_5As_3$ (**3**) are shown to the right. Fe-centered As_4 tetrahedra are shown as blue polyhedra, while Fe-centered As_5 square pyramids in $CaFe_2As_2$ are drawn with Fe–As bond connections. Calcium, iron and arsenic atoms are drawn as red, blue and open circles, respectively.

was checked for purity via powder X-ray diffraction (Figure S1 Supp. Information). In the next step Ca, As and FeAs (14:9.9:1.1) with a total sample weight of 0.5 g were placed in a graphitized silica tube and heated in a muffle furnace. The ampoule was heated to 1325 K in 6 h, held at this temperature for 48 h and then cooled to 1073 K in 42 h. After 24 h at 1073 K the ampoule was cooled to room temperature with a rate of 4.5 K/min.

The ampoule was opened in the glove box, and capillaries (Hilgenberg GmbH, 0.3 mm inner diameter) were prepared for powder X-ray diffraction analysis on a Stoe StadiP diffractometer with Ge (111) monochromized Cu-$K_{\alpha1}$ radiation (1.54056 Å). As an external standard Si was used. The powder X-ray diffraction pattern (Figure S2, Supp. Information) showed the presence of $Ca_{14}FeAs_{11}$ as the main phase, the additional reflexes belong to a new binary phase $Ca_{11}As_{10}$.[26] The tetragonal lattice parameters were obtained from least-square fits of the powder data of $Ca_{14}FeAs_{11}$ using WinXPOW.[27] The sample showed high sensitivity towards air and moisture.

Structure determination. Single crystal X-ray diffraction was performed with an Oxford Diffractions Xcalibur 3 instrument with graphite-monochromatized Mo-K_α radiation (0.71071 Å) at 150 K under a constant N_2 flow. An empirical absorption correction was applied.[28] The starting atomic parameters for $Ca_{14}FeAs_{11}$ were deduced from an automatic interpretation of Direct Methods with SHELXS-2014.[29] The structure was then refined using SHELXL-2014 (full-matrix least-square on F_o^2)[30] with anisotropic atomic displacement parameters for all atoms. The occupancy parameters for each atom were refined in separate least-squares cycles to check the correct composition of the compound. The refinements showed that all atom sites are fully occupied, but the isotropic equivalent displacement parameter of the central As4 position of the $[As_3]^{7-}$ unit is almost 3 times larger than that for the other atomic positions. The displacement ellipsoid is elongated along the As–As–As bond axis. Therefore, the Wyckoff position 8*b* of As4 was split into 16*f* with an occupancy of 50 %. A similar approach was performed e. g. by Kim *et al.* for compound $Ca_{14}MnP_{11}$.[7] In Table 2 both, the Wyckoff position 8*b* as well as the Wyckoff position 16*f* with their respective isotropic equivalent displacement parameters are given. The presence of Nb in the single crystals can be ruled out, since the diffractogram of FeAs precursor shows no Nb containing phases and the subsequent synthesis step was performed in graphitized quartz ampoule. The refinements of the single crystal X-ray diffraction data of the TAs_4 tetrahedra show an *T* occupancy of ~100 % for *T* = Fe and a significant lower value for *T* = Nb. Further details of the crystal structure investigation may be obtained from the Cambridge Crystallographic Data Centre, CCDC, 12 Union Road, Cambridge CB21EZ, UK (Fax: +44-1223-336-033; E-mail: deposit@ccdc.cam.ac.uk) on quoting the depository number CSD- 2169648.

Electronic Structure Calculations. The linear muffin-tin orbital (LMTO) method in the atomic sphere approximation (ASA) using the tight-binding (TB) program TB-LMTO-ASA[31] was employed to analyze the electronic structure of $Ca_{14}FeAs_{11}$. The radii of the muffin-tin spheres were determined after Jepsen and Andersen.[32] The following valence functions were used for the basis set for the short-ranged atom-centered TB-LMTOs: s-d valence functions for Ca, s-d valence functions for Fe and s, p valence functions for As. Ca 4p orbitals were treated by the downfolding technique.[33] The atomic position of As at the center position of the $[As_3]^{7-}$ unit was 8*b* with full occupation. The density of state (DOS) analysis has been done for partial and total DOS of $Ca_{14}FeAs_{11}$ including the iDOS.

Results and Discussions

Synthesis

All attempts to synthesize $Ca_{14}FeAs_{11}$ directly from the elements resulted in a mixture of the ternary $CaFe_2As_2$ and the binary Ca–As phases. Therefore, we applied the two-step procedure by alloying first the p-block and transition metal followed by the reaction of the alloy with the alkaline earth metal, which was introduced by our group before.[34]

Crystal structure

$Ca_{14}FeAs_{11}$ crystallizes with the structure type $Ca_{14}AlSb_{11}$ in the space group $I4_1/acd$ (no.142, $Z = 8$). The crystal structure of this family has recently been discussed in detail,[1,2,5,7,10,11] and thus, only the most important structural features will be mentioned here. The crystallographic data and structural parameters are shown in Tables 1–3. $Ca_{14}FeAs_{11}$ represents the first Fe-containing compound in the series $Ae_{14}TPn_{11}$. The unit cell contains isolated $FeAs_4$ tetrahedra, linear $[As_3]$ units and isolated As and Ca atoms in the ratio 1:1: 4 :14 and with $Z = 8$ in total 112 Ca atoms, eight $[As_3]$ units, eight $FeAs_4$ units and 32 isolated As atoms per unit cell (Figure 2).

The lattice parameters of $Ca_{14}FeAs_{11}$ are comparable with those of the homologous compounds $Ca_{14}MnP_{11}$,[7] $Ca_{14}MnAs_{11}$ and $Ca_{14}MnSb_{11}$.[4] As expected, this series shows an increase of cell parameters with the increasing size of the *Pn* atoms (Table 4). The $a = b$ parameters increase from 15.33 to 15.71 to 16.69 Å for the phosphide, arsenide and the antimonide, respectively and the *c* parameter from 20.76 to 21.14 to 22.27 Å, respectively. Substitution of Mn in $Ca_{14}MnAs_{11}$ with Fe results in a slight decrease of the unit cell parameters in accordance with

Table 1. Crystal data and structure refinement for $Ca_{14}FeAs_{11}$.

Empirical formula	$Ca_{14}FeAs_{11}$
Formula weight/g mol^{-1}	1441.09
Space group, *Z*	$I4_1/acd$, 8
Unit cell dimensions/Å	$a = 15.6268(2)$
	$c = 20.9781(5)$
	$V = 5122.8(2)$ Å^3
Calculated density/g cm^{-3}	3.737
Absorption coefficient/mm^{-1}	17.486
F(000)/e	5352
Crystal size/mm	0.2 × 0.1 × 0.07
θ range/deg	3.07 to 32.88
Range in *hkl*	$\pm 23\ h$, $-23 \le k \le 19$, $\pm 31\ l$
Reflections collected	45417
Independent reflections	2344 ($R_{int} = 0.074$)
Reflections with $I \ge 2\sigma(I)$	1604 ($R_\sigma = 0.042$)
Data/parameters	2344/64
GOF on F^2	0.990
Final *R* indices [$I \ge 2\sigma(I)$]	$R_1 = 0.034$
	$wR_2 = 0.071$
R indices (all data)	$R_1 = 0.058$
	$wR_2 = 0.079$
Largest diff. peak and hole/e·Å^{-3}	1.479 and −1.486

Table 2. Atomic coordinates, isotropic equivalent displacement parameters (/Å^2·10^3, space group $I4_1/acd$, $Z=8$).

Atom	Occupancy	Wyckoff position	*x*	*y*	*z*	U_{eq}
Ca1	1	32 *g*	0.02344(5)	0.37785(5)	0.00522(4)	11.5(2)
Ca2	1	32 *g*	0.04333(5)	0.07339(5)	0.17140(4)	11.0(2)
Ca3	1	32 *g*	0.34344(6)	0.07035(6)	0.09278(4)	13.0(2)
Ca4	1	16*e*	0.35305(8)	0	1/4	10.3(2)
Fe	1	8*a*	0	1/4	3/8	11.3(2)
As1	1	32 *g*	0.13002(3)	0.02566(3)	0.04681(2)	10.1(2)
As2	1	32 *g*	0.36525(3)	0.25405(3)	0.06057(2)	10.0(2)
As3	1	16*f*	0.13438(3)	0.38438(3)	1/8	9.5(2)
As4	1	8*b*	0	1/4	1/8	26.5(3)
As4[#]	*0.5*	*16f*	*0.00879(14)*	*0.25879(14)*	*1/8*	*11.3(7)*

[#] Alternative split position refinement.

Table 3. Interatomic distances (*d*) within the first coordination sphere including their multiplicity for the individual structural units of $Ca_{14}FeAs_{11}$, space group $I4_1/acd$, $Z=8$.

Atom1 Isolated As^{3-}	Atom2	*d*/Å	Atom1 $[As_3]^{7-}$ unit	Atom2	*d*/Å	Atom1 $FeAs_4$ unit	Atom2	*d*/Å
As1	–Ca4	2.920(1); ×1	As3	–Ca3	3.004(2); ×2	Fe1	–As2	2.503(1); ×4
	–Ca1	2.964(1); ×1		–Ca4	3.190(1); ×2	As2	–Ca1	2.945(1); ×1
	–Ca2	2.996(1); ×1		–As4	2.776(3); ×1		–Ca3	2.969(1); ×1
	–Ca2	3.037(1); ×1		–As4	3.164(3); ×1		–Ca2	3.063(1); ×1
	–Ca3	3.039(1); ×1		–Ca2	3.016(1); ×2		–Ca2	3.082(1); ×1
	–Ca1	3.050(1); ×1		–Ca1	3.055(1); ×2		–Ca4	3.138(1); ×1
	–Ca3	3.071(1); ×1	As4(16*f*)	–Ca2	2.914(3); ×2		–Ca3	3.207(1); ×1
	–Ca3	3.541(2); ×1		–Ca2	3.104(3); ×2		-Ca1	3.502(1); ×1
				–Ca1	3.135(2); ×2			
				–Ca1	3.356(2); ×2			

the smaller covalent radius of Fe,[35] but has a drastic effect on the tetrahedral [TAs_4] units.

The distance between the transition metal and the four surrounding As atoms decreases from 2.60 Å in $Ca_{14}MnAs_{11}$ to 2.503(1) Å in $Ca_{14}FeAs_{11}$, and the Fe–As distance is in agreement with a covalent bond. The tetrahedral $FeAs_4$ unit is flattened in the *ab* plane, resulting in a distortion expressed by two different As–Fe-As angles of 106.95(1) and 114.64(2)° which deviate considerably from the ideal value of 109.4°. The distortion of the tetrahedra in $Ca_{14}MnAs_{11}$ with angles of 107.5° and 114.4° has been attributed to a *Jahn-Teller* effect of the Mn-d^4 atoms.[3,4,7,9,15,16] However, in $Ca_{14}FeAs_{11}$ the tetrahedra are even slightly more distorted, although the isovalent Fe atoms in $Ca_{14}FeAs_{11}$ most probably correspond to a *hs*-d^5 configuration (Fe^{3+}) for which no *Jahn-Teller* distortion is expected.

In this context it is interesting to compare the structure parameters of $Ca_{14}FeAs_{11}$ with those of analogous compounds that exclusively contain main group elements. In $Ca_{14}GaAs_{11}$ the two angles of the distorted tetrahedra are 107.8° (α) and 113.0° (β), and thus the tetrahedra are also distorted without any electronic reason. Due to the very similar covalent radii of Ga and Fe (1.26 and 1.24 Å, respectively)[35] the cell parameters of $Ca_{14}GaAs_{11}$ and $Ca_{14}FeAs_{11}$ are also very similar. The *a* axes are almost identical, whereas the *c* axis of the Ga compound is slightly longer by 0.16 Å (Table 4). The difference in the *c* axis is also reflected by longer Ga–As bonds (2.55 Å) if compared to the Fe–As bonds (2.5030(5) Å). Rather similar structural parameters of TAs_4 tetrahedra occur for isostructural but defect variants $Sr_{13}NbAs_{11}$ and $Eu_{13}NbAs_{11}$, with Nb–As bond lenghts of 2.51 Å for both structures and the bond angles of the distorted tetrahedra of 107.1° (α) and 114.2° (β) for $Sr_{13}NbAs_{11}$ and 107.1° (α) and 114.4° (β) for $Eu_{13}NbAs_{11}$.[36]

Each As atom of the $FeAs_4$ unit in $Ca_{14}FeAs_{11}$ is coordinated by three terminal Ca atoms (Ca2, Ca4) and four Ca atoms (Ca1, Ca3) that bridge the four edges of the tetrahedra within the first coordination sphere (Figure 3). As a result, the $FeAs_4$ unit is surrounded by 20 Ca atoms; the distances between the As atoms and the surrounding Ca atoms are listed in Table 3. The size of the cations affects the interatomic distances within the TPn_4 motif (and all the other structural motifs). A comparison between $Yb_{14}MnSb_{11}$,[11] $Ca_{14}MnSb_{11}$, $Sr_{14}MnSb_{11}$, and $Ba_{14}MnSb_{11}$[4] reveals that the distance $d_{Mn–Sb}$ increases steadily with the ionic size of the cation. The same trend holds for the isostructural Bi compounds (Table 4).[3,11]

As second type of anion, linear $[As_3]^{7-}$ polyanions, are located between the $FeAs_4$ units with As3 and As4 as the terminal and central atoms, respectively (Figure 4). The refinement of the single crystal data show a noticeable increase of displacement parameters of As4 towards the adjacent terminal As3 atoms (Figure 4a), and thus the refinement of two split

Table 4. Lattice parameters, *c/a* values and interatomic distances of selected compounds $A_{14}TPn_{11}$ (*A* = alkaline earth, rare earth metals, *T* = main group or transition metal elements, *Pn* = pnictide elements; space group $I4_1/acd$, Z = 8).

Compound	*a*/Å	*c*/Å	*V*/Å^3	*c/a*	$d_{T\text{-}Pn}$/ Å	$d_{Pn\text{-}Pn}$ */ Å	Ref
Pn = P							
$Ca_{14}GaP_{11}$	15.35	20.76	4890	1.35	2.54	2.93	[6]
$Ca_{14}MnP_{11}$	15.33	20.76	4875	1.35	2.54	2.93	[7]
$Ba_{14}InP_{11}$	17.10	22.94	6706	1.34	2.71	3.19	[19]
$Eu_{14}MnP_{11}$	15.93	21.21	5383	1.33	2.59	3.06	[9]
Pn = As							
$Ca_{14}GaAs_{11}$	15.62	21.14	5157	1.35	2.55	2.96	[5]
$Ca_{14}MnAs_{11}$	15.71	21.14	5220	1.35	2.60	3.18	[4]
$Ca_{14}FeAs_{11}$	15.6268(2)	20.9781(5)	5122.8(2)	1.342	2.5030(5)	2.9697(5)	This work
$Sr_{14}GaAs_{11}$	15.62	21.14	5157	1.35	2.55	2.96	[5]
$Sr_{14}Zn_{1.33}As_{11}$	16.52	22.19	6055	1.34	2.66	3.15	[40]
$Sr_{13}NbAs_{11}$	16.50	22.14	6026	1.34	2.51	3.09	[36]
$Sr_{14}MnAs_{11}$	16.58	22.17	6091	1.34	2.68	3.15	[4]
$Eu_{14}Zn_{1.14}As_{11}$	16.27	21.69	5742	1.33	2.63	3.04	[40]
$Eu_{13}NbAs_{11}$	16.33	21.97	5859	1.35	2.51	3.05	[36]
Pn = Sb							
$Ca_{14}AlSb_{11}$	16.68	22.42	6236	1.35	2.72	3.20	[1]
$Ca_{14}MnSb_{11}$	16.69	22.27	6201	1.33	2.76	3.22	[4]
$Ca_{14}MgSb_{11}$	16.69	22.58	6291	1.35	2.81	3.22	[21]
$Sr_{14}AlSb_{11}$	17.50	23.48	7185	1.34	2.83	3.30	[2]
$Sr_{14}MnSb_{11}$	17.51	23.32	7151	1.33	2.84	3.31	[4]
$Ba_{14}AlSb_{11}$	18.29	24.22	8105	1.32	2.80	3.37	[2]
$Ba_{14}MnSb_{11}$	18.39	24.07	8144	1.31	2.87	3.42	[4]
$Eu_{14}InSb_{11}$	17.29	22.77	6608	1.32	2.87	3.26	[16]
$Yb_{14}MnSb_{11}$	16.62	21.95	6059	1.32	2.75	3.20	[11]
$Yb_{14}ZnSb_{11}$	16.56	21.86	5996	1.32	2.73	3.18	[41]
$Yb_{14}MgSb_{11}$	16.63	22.24	6145	1.34	2.81	3.20	[21]
Pn = Bi							
$Ca_{14}MnBi_{11}$	17.07	22.50	6553	1.32	2.81	3.34	[3]
$Sr_{14}MnBi_{11}$	17.85	23.44	7454	1.31	2.89	3.43	[3]
$Ba_{14}MnBi_{11}$	18.67	24.43	8511	1.31	2.94	3.50	[3]
$Yb_{14}MnBi_{11}$	17.00	22.26	6433	1.31	2.80	3.34	[11]

* d_{Pn-Pn} – distances between the two *Pn* atoms forming the $[Pn_3]^{7-}$ unit with non-split 8*b* Wyckoff position.

positions for As4, each occupied by 50 %, is recommended (Figure 4b). As a result the As4 position is shifted by 0.0088(2) Å in the *x/y* direction towards Wyckoff position 16*f*. This splitting leads to two different As–As distances of 2.776(3) and 3.164(3) Å (Figure 4c) and to smaller displacement parameters. The shorter As3–As4 bond of 2.776(3) Å is still longer than the covalent As–As bonds in elemental As (2.44 –2.52 Å)[35] and in binary Ca–As compounds (2.47 –2.57 Å),[37–39] but somewhat shorter than that observed for the collapsed $CaFe_2As_2$ phase (2.86 Å).[22]

As shown in Table 4, there exist many isostructural compounds. In the aristo-type $Ca_{14}AlSb_{11}$ a symmetric linear unit with equivalent Sb–Sb distances $d_{Sb3-Sb4}$ of 3.20 Å and the central atom on the special atomic Wyckoff position 8*b* (0, $^1/_4$, $^1/_8$) have been reported.[1] The same holds for isotypic $Ca_{14}GaAs_{11}$, that, however, shows a strongly elongated displacement ellipsoid of the central As atom.[5] Isostructural compounds containing P all show a noticeable enlargement of the anisotropic displacement parameters of the central atom,[6,7,9,19] and the authors described the $[P_3]^{7-}$ unit alternatively as $[P_2]^{4-}$ dumbbells linearly coordinated to isolated P^{3-} atoms by implementing split positions.

Within the first coordination sphere the $[As_3]^{7-}$ unit is surrounded by 16 Ca atoms. Four Ca atoms are bridging the As–As bonds, resulting in the formation of two distorted, vertex-sharing "Ca_4As_2" octahedra (Figure 4b). The other eight Ca atoms are terminally coordinated to the As3 atoms (four on each side). The atomic distances are listed in Table 2.

The isolated As^{3-} anions (As1) are coordinated by eight Ca^{2+} cations in the form of a distorted trigonal prism with two capped faces (Figure 5). The trigonal-prismatic coordination of Ca around As is also observed in binary Ca–As phases such as Ca_2As_3.[37] The distances between As1 and Ca are between 2.920(1) and 3.541(1) Å. In $Ca_{14}GaAs_{11}$, distances between 2.92 and 3.56 Å are observed, which again proves the similarity of the two isostructural compounds.

In the phosphides $Ae_{14}TP_{11}$ the P–P distance in the polyanion is mainly dominated by the size of the *Ae* atoms. For the arsenides $Ca_{14}GaAs_{11}$ and $Ca_{14}FeAs_{11}$ the same As–As distance of 2.96 and 2.97 Å, respectively, is found and in $Sr_{14}MnAs_{11}$, the expected longer distance of 3.15 Å is observed, however, in $Ca_{14}MnAs_{11}$ the longest distance of 3.18 has been reported despite the presence of the smaller Ca atom (Table 4).

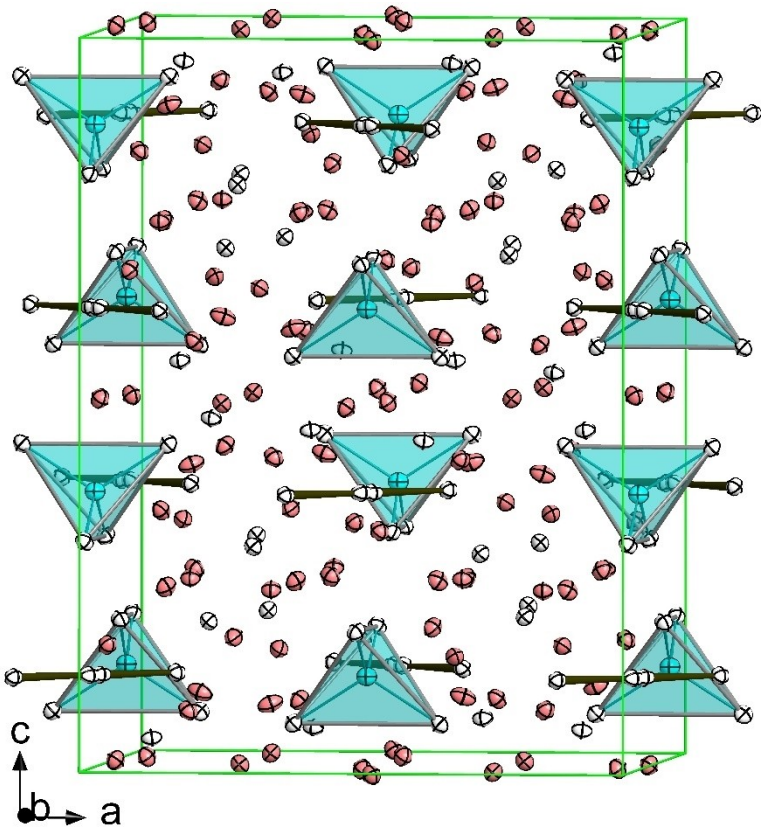

Figure 2. The unit cell of the structure of $Ca_{14}FeAs_{11}$. Atoms are represented as ellipsoids with a 75% probability level (Ca - red, Fe - blue and As - white). Covalent Fe–As bonds are shown in blue, As–As bonds in dark gray, and $FeAs_4$ tetrahedra are drawn in blue.

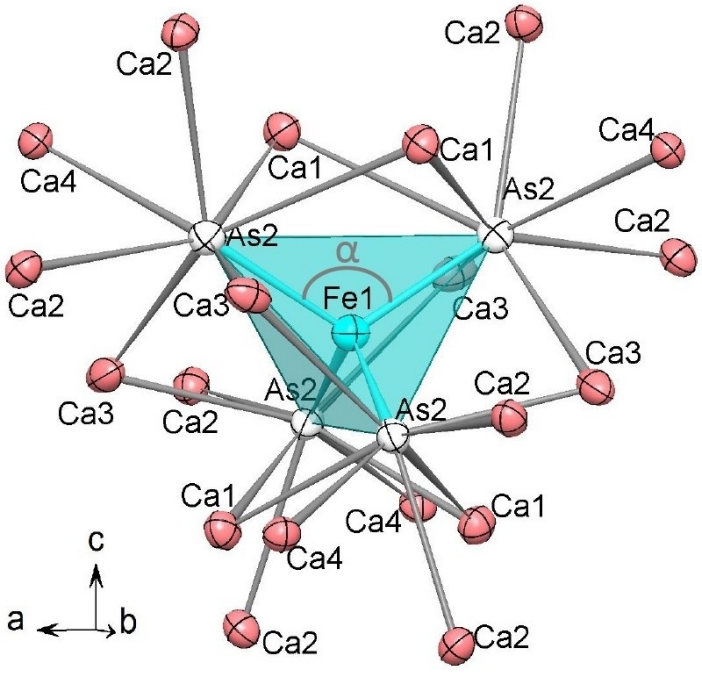

Figure 3. The Ca environment of the $FeAs_4$ tetrahedron is shown. The atoms are drawn as ellipsoids with a 75% probability level. The As–Fe-As angle α is marked.

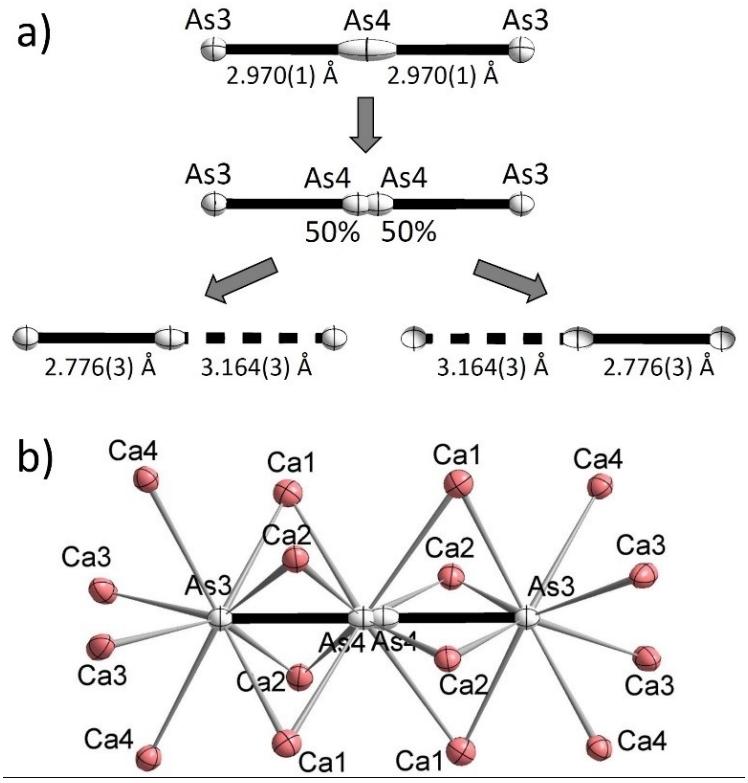

Figure 4. Representation of the disordered $[As3]^{7-}$ unit. a) The unit with As4 on Wyckoff position 8*b* with 100% occupation with equal As3–As4 distances (structure model 1). Model 2 with split 50%/50% positions of As4 (b), which can be interpreted as statistical mixture of two ordered variants (c). Coordination of the $[As_3]^{7-}$ unit by Ca^{2+} cations (d). The atoms are shown as ellipsoids with a 90% probability level.

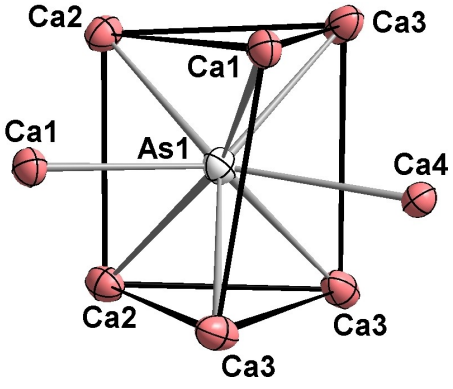

Figure 5. Coordination of the As1 atom. The atoms are shown as ellipsoids with a 75% probability level. Ca–As bonds are drawn in gray, Ca–Ca contacts in black (non-covalent and only for visible clarification).

Electronic structure of $Ca_{14}FeAs_{11}$

Assuming a salt-like charge allocation for Zintl phases in $Ca_{14}FeAs_{11}$, the electropositive Ca atoms carry a charge of +2 per atom, resulting in 28 positive charges per formula unit, and discrete As atoms with a charge of 3- give a total of $4\times3=12$ negative charges. In analogy to the known linear polyanion I_3^-, the iso(valence)-electronic linear As_3 arises as a $[As_3]^{7-}$ polyanion. Thus, for a charge-balanced compound, a charge of −9 (+28−7−12 = 9) is needed for the $FeAs_4$ tetrahedra, which can easily be rationalized by a formal charge of 3− for the As atoms and 3+ for the centering Fe atom, resulting in $[FeAs_4]^{9-}$. Thus, $Ca_{14}FeAs_{11}$ can be rewritten as $(Ca^{2+})_{14}[(As^{3-})_4]([As_3]^{7-})([FeAs_4]^{9-})$.

In order to analyze the electronic structure of $Ca_{14}FeAs_{11}$, total and partial DOS were calculated. The structural parameters obtained from the single crystal refinement were used, with the central position (As4) of the $[As_3]^{7-}$ unit centered between the As4 atoms (space group $I4_1/acd$). Using an asymmetric central As atom according to the split position by applying a superstructure model did not lead to significant changes in the DOS therefore we did not further consider this model. Figure 6 shows the partial DOS for Fe-d (turqois), Ca-d (gray), As-s,p of the $FeAs_4$ unit (magenta), and As-s,p of the As_3 unit (green). For the total DOS (black curves) five blocks of energy levels that are separated by energy gaps are observed. The block at lowest energies is between −12 and −9.5 eV, followed by a gap of approximately 5 eV. The main contribution in the block arises from the As-s,p orbitals of the $FeAs_4$ and the As_3 units (the As-s orbitals are the most dominant contributors, the corresponding pDOS is not shown). The second block is located between −4.5 and −0.5 eV. All atoms of the presented pDOSs have contributions in this block, but the main contribution in the block arises

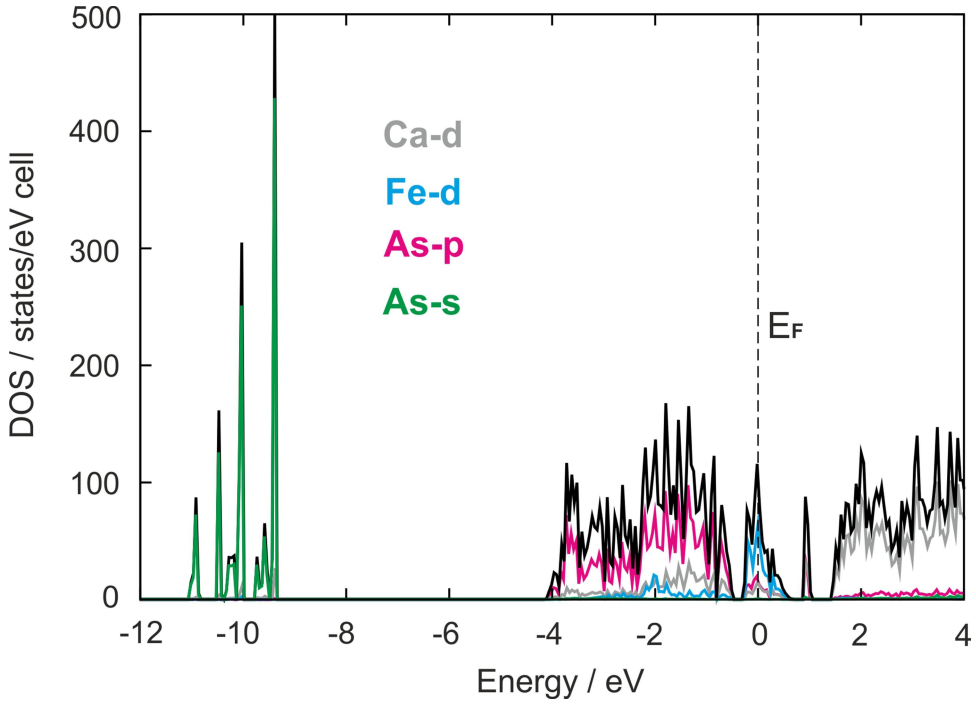

Figure 6. DOS and partial DOS of $Ca_{14}FeAs_{11}$: non-split atom model (space group $I4_1/acd$). Total DOS (black) including pDOS of Fe-d (turquois), As-p (magenta), As-s (green) and Ca-d (gray).

from the As-s orbitals. Around the Fermi level, between −0.5 and 0.6 eV, the main contributions are attributed to Fe-d orbitals with input from As-p orbitals of the $FeAs_4$ unit and Ca-d orbitals. Since the course of the pDOS curve of the Fe-d orbitals reflects those of the As-p orbitals, orbital mixing is anticipated. The strong interactions of the orbitals correspond to the covalent bonds between Fe and As within the isolated tetrahedra. Since all contributions originate from Fe-d and As-p orbitals of the $FeAs_4$ unit, the Ca-d contributions in this block are most likely due to Ca atoms coordinating the tetrahedra. At the Fermi level the DOS shows a local maximum. The presence of a considerable amount of states at the Fermi level indicates metallic behavior. Above 0.9 eV the main contributions arise from the Ca-d orbitals.

In addition, the band structure, including fat bands of Fe-d orbitals, and the Crystal Orbital Hamilton Population (COHP) for the Fe–As bond were investigated (Figure 7). The COHP for the Fe–As bond (2.503 Å) including the iCOHP is shown in Figure 7. At energies below −9 eV the bonding states of the As-s orbitals are present, the iCOHP value is low for the block. Between approximately −4.2 and −0.4 eV a second block of bonding states is present. From pDOS the states represent mainly As-p and some Fe-d orbitals, thus pointing for bonding Fe–As interactions. The block of states in DOS around the Fermi level (−0.4 eV and 0.8 eV) show anti-bonding character with some As-p and mainly Fe-d orbital contributions. The iCOHP value at the Fermi level has a value of 2.66 eV, which confirms the covalent bonding interaction within the isolated $FeAs_4$ tetrahedra.

Fe-d orbitals in a tetrahedral environment are split into e_g, with two degenerated states at lower energies, and t_{2g}, with three degenerated states at higher energies. To find out, whether the e_g and t_{2g} states in $Ca_{14}FeAs_{11}$ are of bonding or anti-bonding character and where the states are located, the fat bands for the 5 Fe-d orbitals have been calculated. The Fe-d fat bands for $Ca_{14}FeAs_{11}$ between −0.4 and 0.8 eV are depicted in Figures 9b-9f. The anti-bonding COHP region between −0.4 and 0.8 eV also shows fat band contributions from the Fe-d orbitals. For the tetragonal space group $I4_1/acd$, the Γ k-point lies in the origin of the Brillouin zone, and therefore the fat band distribution of the Fe-d orbitals at Γ is compared. A clear distinction between the different Fe-d orbitals can be made. Fe-d_{xy} and Fe-d_{z^2} has fat band contributions mainly located below the Fermi level (Figure 8). The Fe-d_{xz}, Fe-d_{yz} and Fe-$d_{x^2-y^2}$ fat band contributions are above the Fermi level. At the Fermi level all Fe-d orbitals show contributions. This distribution of the Fe-d fat bands reflects the expected e_g and t_{2g} states for Fe in a tetrahedral environment. However, Fe-$d_{x^2-y^2}$ is located in the higher energy t_{2g} state, while Fe-d_{xy} appears in the lower energy e_g state, which can be explained by a 45° rotation of the unit cell around the c axis for the non-split atom model. In conclusion, as known for molecular units, the Fe-d states of the Fe–As interactions are anti-bonding in character at the Fermi level and are also separated in e_g and t_{2g} levels.

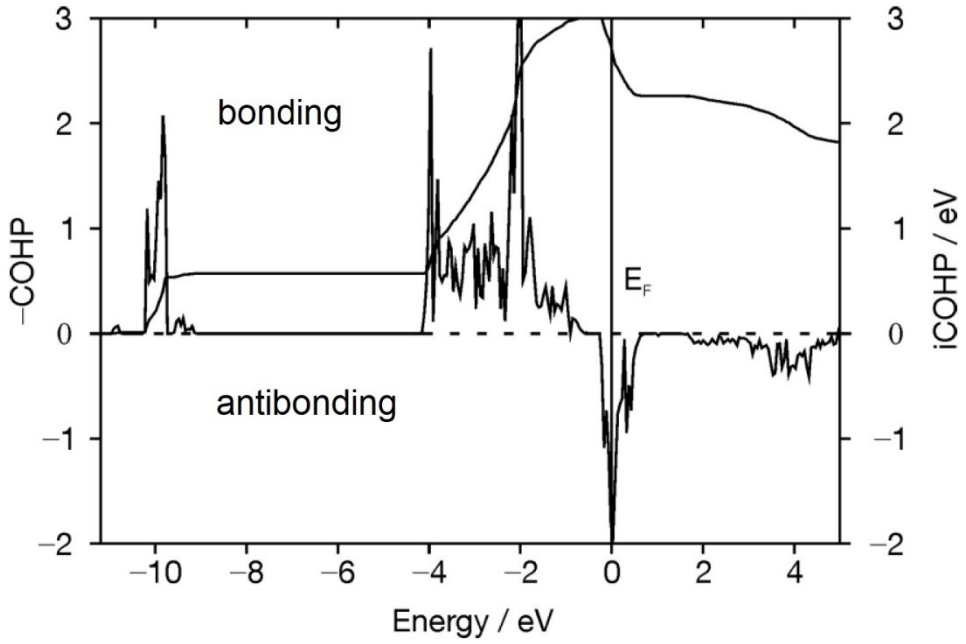

Figure 7. COHP and iCOPH of the Fe–As bond in $Ca_{14}FeAs_{11}$ (non-split atom model).

Conclusions and Discussion

The intermetallic compound $Ca_{14}FeAs_{11}$ is the first compound in its respective group of *A-T-Pn* (*A* = alkaline earth-, rare earth-metal; *T* = Mg, group 13 element, transition metal; *Pn* = pnictide element) with Fe as the transition metal. This finding is most interesting since reports on composites of Fe and $Yb_{14}MgSb_{11}$ do not incorporated Fe even on mechanical milling and spark plasma sintering procedure.[42] The structure of $Ca_{14}FeAs_{11}$ combines the structural motifs observed in binary Ca–As phases[37–39] on the one hand and in binary Fe–As and ternary Ca–Fe–As phases[22–24] on the other. $FeAs_4$ tetrahedra are observed in Fe_2As and in all ternary Ca–Fe–As compounds. In the previously reported binary Fe–As phases the tetrahedra are exclusively edge-sharing, while $Ca_{14}FeAs_{11}$ contains only isolated $FeAs_4$ tetrahedra. Furthermore, the compound also contains linear As_3 units which can be described as As–As dimers that coordinate to a further As atom. As–As dumbbells are also observed in binary Ca–As Zintl phases.[39] The dumbbell atoms are coordinated by eight Ca atoms forming a distorted square anti-prism with one square face capped by a covalently bonded As atom of the dumbbell and second square face capped by an isolated As atom. The Ca content in $Ca_{14}FeAs_{11}$ is approximately 53.8 at.% and falls into the composition range of binary Ca–As compounds, in which dumbbells of As atoms occur. In all cases, the coordination around the dumbbells is very similar. In an alternative description, the As_3 unit consist of three covalently connected As atoms, that well known in the chemistry of main group elements, e.g. in XeF_2 and in the anions IF_2^- or I_3^-. In case of equal As–As distances, the central atom As4 of the As_3-unit has 5 electron pairs, which, according to the Gillespie/Nyholm concept, are arranged in a trigonal bipyramid with the non-bonding electron pairs located in the equatorial plane and the two As ligand atoms occupying the axial positions, leading to the observed linear As_3 anion.

The structural motif of $FeAs_4$ tetrahedra is very prominent in the class of iron-pnictide superconductors,[43] and the superconducting behavior of these materials is assumed to be associated with the layers of condensed $FeAs_4$ tetrahedra and the structure of the tetrahedra within these layers have a big influence on the superconducting properties. The tetrahedra are connected by shared edges forming either 2D-layers or in some cases 3D-networks.[43,44] It has formerly been stated that compounds with close to ideal tetrahedral angles have the highest critical temperatures (T_c).[45] Lately it has been argued that not the angles but the height between the square *T* layer and the adjacent *Pn* layer (h_{T-Pn}) is more important for the T_c.[46] $CaFe_2As_2$ ($ThCr_2Si_2$ structure type, $a = 3.87$ Å and $c = 11.73$ Å)[47] is not superconducting under normal conditions, but superconductivity can be induced by pressure[22] or by doping.[48] In $CaFe_2As_2$ the tetrahedra are only slightly distorted (tetrahedral angles are 109.4° and 109.5°), whereas the distortion of the tetrahedra in the title compound is larger.

The oxidation state of Fe in the tetrahedra can be either +2 or +3, resulting in $[FeAs_4]^{9-}$ or $[FeAs_4]^{10-}$ units, respectively. Fe^{3+} has a d^5 electron configuration, and thus the tetrahedra are expected to show no *Jahn-Teller* distortion. For an oxidation state +2 and a d^6 electron configuration a distortion for the tetrahedra is expected. The tetrahedra in $Ca_{14}FeAs_{11}$ are weakly distorted, but distorted $FePn_4$ tetrahedra with Fe^{3+} do also exist, such as for example in Na_5FeS_4, which contains isolated FeS_4 tetrahedra with angles between 106.6 and 113.1°.

The isolated TE_4 units are distorted in all compounds, with the tetrahedra flattened along the *c* axis. The strongest

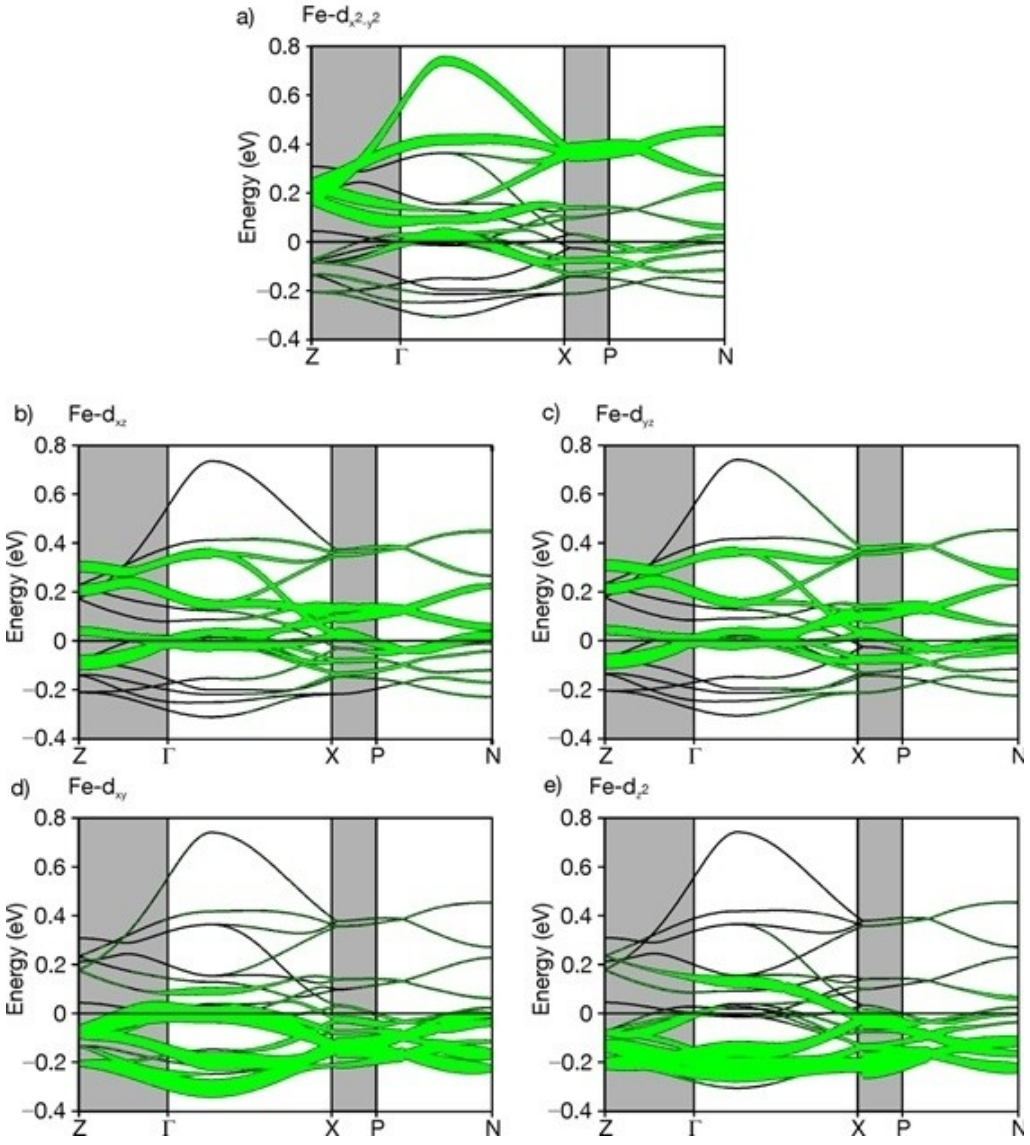

Figure 8. Electronic structure of $Ca_{14}FeAs_{11}$ (non-split atom model). (a) COHP for Fe–As bond ($d_{Fe-As} = 2.503$ Å); fat bands for b) Fe-$d_{x^2-y^2}$, c) Fe-d_{xz}, d) Fe-d_{yz}, e) Fe-d_{xy} and f) Fe-d_{z^2}; *k*-paths parallel to the *c* direction are highlighted in gray, path parallel to the *ab* plane in white.

distortion is observed for the Mn compounds and is attributed to a d^4 *Jahn-Teller* distortion. In most of these compounds the *T* element has the oxidation state 3+ which has been confirmed by magnetic measurements.[2,4–6,15,17,19] Kauzlarich *et al.* have shown that $Ca_{14}MnP_{11}$ displays a paramagnetic moment most consistent with an oxidation state of +2 on the Mn site, and in this case the tetrahedra are less distorted.[7] However, since the $GaAs_4$ tetrahedra in $Ca_{14}GaAs_{11}$ are also distorted, ion packing effects may play a major role for the structural distortion. Since the Fe content of the title compound $Ca_{14}FeAs_{11}$ is rather low, and since the compound is air-sensitive and elemental iron impurities cannot be excluded, Mössbauer spectroscopy failed to conclusively determine the oxidation state of Fe. Furthermore, the compound was not obtained as a phase-pure material but with binary $Ca_{11}As_{10}$ as an impurity, and therefore magnetic measurements did also not lead to a conclusive determination of the oxidation state of Fe in the title compound.

Acknowledgements

The Authors would like to thank the German Research Foundation (Deutsche Forschungsgemeinschaft, DFG, Grant HL 62/3-1) for financial support. Open Access funding enabled and organized by Projekt DEAL.

Conflict of Interest

The authors declare no conflict of interest.

[1] G. Cordier, H. Schäfer, M. Stelter, *Z. Anorg. Allg. Chem.* **1984**, *519*, 183–188.
[2] S. L. Brock, L. J. Weston, M. M. Olmstead, S. M. Kauzlarich, *J. Solid State Chem.* **1993**, *107*, 513–523.
[3] T. Y. Kuromoto, S. M. Kauzlarich, D. J. Webb, *Chem. Mater.* **1992**, *4*, 435–440.
[4] A. Rehr, T. Y. Kuromoto, S. M. Kauzlarich, J. Del Castillo, D. J. Webb, *Chem. Mater.* **1994**, *6*, 93–99.
[5] S. M. Kauzlarich, M. M. Thomas, D. A. Odink, M. M. Olmstead, *J. Am. Chem. Soc.* **1991**, *113*, 7205–7208.
[6] J. T. Vaughey, J. D. Corbett, *Chem. Mater.* **1996**, *8*, 671–675.
[7] H. Kim, S. M. Kauzlarich, *J. Solid State Chem.* **2005**, *178*, 1935–1939.
[8] H. Kim, Q. Huang, J. W. Lynn, S. M. Kauzlarich, *J. Solid State Chem.* **2002**, *168*, 162–168.
[9] A. C. Payne, M. M. Olmstead, S. M. Kauzlarich, D. J. Webb, *Chem. Mater.* **2001**, *13*, 1398–1406.
[10] Y. Hu, G. Cerretti, E. L. Kunz Wille, S. K. Bux, S. M. Kauzlarich, *J. Solid State Chem.* **2019**, *271*, 88–102.
[11] J. Y. Chan, M. M. Olmstead, S. M. Kauzlarich, D. J. Webb, *Chem. Mater.* **1998**, *10*, 3583–3588.
[12] A. P. Holm, T. C. Ozawa, S. M. Kauzlarich, S. A. Morton, G. Dan Waddill, J. G. Tobin, *J. Solid State Chem.* **2005**, *178*, 262–269.
[13] H. Kim, P. Klavins, S. M. Kauzlarich, *Chem. Mater.* **2002**, *14*, 2308–2316.
[14] H. Kim, M. M. Olmstead, P. Klavins, D. J. Webb, S. M. Kauzlarich, *Chem. Mater.* **2002**, *14*, 3382–3390; C. A. Cox, E. S. Toberer, A. A. Levchenko, S. R. Brown, G. J. Snyder, A. Navrotsky, S. M. Kauzlarich, *Chem. Mater.* **2009**, *21*, 1354–1360; S. Kastbjerg, C. A. Uvarov, S. M. Kauzlarich, E. Nishibori, M. A. Spackman, B. B. Iversen, *Chem. Mater.* **2011**, *23*, 3723–3730.
[15] E. Ratai, P. Bruins, C. J. Hernandez, S. M. Kauzlarich, M. P. Augustine, *Chem. Mater.* **2002**, *14*, 2467–2475.
[16] J. Y. Chan, M. E. Wang, A. Rehr, S. M. Kauzlarich, D. J. Webb, *Chem. Mater.* **1997**, *9*, 2131–2138.
[17] J. Y. Chan, S. M. Kauzlarich, P. Klavins, R. N. Shelton, D. J. Webb, *Chem. Mater.* **1997**, *9*, 3132–3135.
[18] S. R. Brown, S. M. Kauzlarich, F. Gascoin, G. J. Snyder, *Chem. Mater.* **2006**, *18*, 1873–1877.
[19] W. Carrillo-Cabrera, M. Somer, K. Peters, H. G. von Schnering, *Chem. Ber.* **1996**, *129*, 1015–1023.
[20] D. M. Young, C. C. Torardi, M. M. Olmstead, S. M. Kauzlarich, *Chem. Mater.* **1995**, *7*, 93–101; M. B. Stone, V. O. Garlea, B. Gillon, A. Cousson, A. D. Christianson, M. D. Lumsden, S. E. Nagler, D. Mandrus, B. C. Sales, *Phys. Rev. B* **2017**, *95*, 020412.
[21] Y. Hu, J. Wang, A. Kawamura, K. Kovnir, S. M. Kauzlarich, *Chem. Mater.* **2015**, *27*, 343–351.
[22] P. C. Canfield, S. L. Bud'ko, N. Ni, A. Kreyssig, A. I. Goldman, R. J. McQueeney, M. S. Torikachvili, D. N. Argyriou, G. Luke, W. Yu, *Physica B + C* **2009**, *469*, 404–412.
[23] I. Todorov, D. Y. Chung, C. D. Malliakas, Q. A. Li, T. Bakas, A. Douvalis, G. Trimarchi, K. Gray, J. F. Mitchell, A. J. Freeman, M. G. Kanatzidis, *J. Am. Chem. Soc.* **2009**, *131*, 5405–5407.
[24] T. Stürzer, C. Hieke, C. Löhnert, F. Nitsche, J. Stahl, C. Maak, R. Pobel, D. Johrendt, *Inorg. Chem.* **2014**, *53*, 6235–6240.
[25] F. Ronning, N. Kurita, E. D. Bauer, B. L. Scott, T. Park, T. Klimczuk, R. Movshovich, J. D. Thompson, *J. Phys. Condens. Matter* **2008**, *20*, 342203; N. Ni, S. Nandi, A. Kreyssig, A. I. Goldman, E. D. Mun, S. L. Bud'ko, P. C. Canfield, *Phys. Rev. B* **2008**, *78*, 014523.
[26] A. Hoffmann, V. Hlukhyy, T. F. Fässler, *Z. Kristallogr. New Cryst. Struct.*, DOI 10.1515/NCRS-2022-0380.
[27] STOE, *WinXPOW*, Version 3.0.2.1 ed., STOE & Cie GmbH, Darmstadt **2011**.
[28] CrysAlis RED, *Scale3/ABSPACK, Version 1.171.33.34d*, *Oxford Diffraction, Poland Sp. z o.o., 2009*.
[29] G. M. Sheldrick, *SHELXS-2014, Program for the Determination of Crystal Structure*, University of Goettingen: Goettingen, Germany, **2014**.
[30] G. M. Sheldrick, *SHELXL-2014, Program for Crystal Structure Refinement*, University of Goettingen: Goettingen, Germany, **2014**.
[31] M. v. Schilfgarde, T. A. Paxton, O. Jepsen, O. K. Andersen, G. Krier, *The Stuttgart Tight-Binding LMTO-ASA program*, Version 4.7 ed., Max-Planck-Institut für Festkörperforschung Stuttgart (Germany), **1998**.
[32] O. Jepsen, O. K. Andersen, *Z. Phys. B* **1995**, *97*, 35–47.
[33] W. R. L. Lambrecht, O. K. Andersen, *Phys. Rev. B* **1986**, *34*, 2439–2449.
[34] S. Stegmaier, T. F. Fässler, *J. Am. Chem. Soc.* **2011**, 19758–19768; S. Stegmaier, T. F. Fässler, *Angew. Chem. Int. Ed.* **2012**, *51*, 1–5; *Angew. Chem.* **2012**, *124*, 1–1; V. Hlukhyy, H. He, L.-A. Jantke, T. F. Fässler, *Chem. Eur. J.* **2012**, *18*, 12000–12007.
[35] A. F. Holleman, N. Wiberg, *Lehrbuch der Anorganischen Chemie*, 102 ed., Berlin, **2007**.
[36] K. Vidyasagar, W. Hönle, H. G. von Schnering, *Z. Anorg. Allg. Chem.* **1996**, *622*, 518–524.
[37] K. Deller, B. Eisenmann, *Z. Naturforsch. B: Chem. Sci.* **1976**, *31*, 1023–1027.
[38] A. Iandelli, E. Franceschi, *J. Less Comm. Metals* **1973**, *30*, 211–216.
[39] A. V. Hoffmann, V. Hlukhyy, T. F. Fassler, *Acta Crystallogr. Sect. E* **2015**, *71*, 1548–1550.
[40] S. Baranets, G. M. Darone, S. Bobev, *J. Solid State Chem.* **2019**, *280*, 120990.
[41] A. P. Holm, T. C. Ozawa, S. M. Kauzlarich, S. A. Morton, G. D. Waddill, J. G. Tobin, *J. Solid State Chem.* **2005**, *178*, 262–269.
[42] C. J. Perez, X. Qi, Z. Chen, S. K. Bux, S. Chanakain, B. Li, K. Liu, R. Dhall, K. C. Bustillo, S. M. Kauzlarich, *ACS Appl. Energ. Mater.* **2020**, *3*, 2147–2159.
[43] A. Chubukov, *Annu. Rev. Condens. Matter Phys* **2012**, *3*, 57–92.
[44] D. C. Johnston, *Adv. Phys.* **2010**, *59*, 803–1061.
[45] C.-H. Lee, A. Iyo, H. Eisaki, H. Kito, M. Teresa Fernandez-Diaz, T. Ito, K. Kihou, H. Matsuhata, M. Braden, K. Yamada, *J. Phys. Soc. Jpn.* **2008**, *77*, 083704.
[46] K. Kuroki, H. Usui, S. Onari, R. Arita, H. Aoki, *Phys. Rev. B* **2009**, *79*, 224511.
[47] G. Wu, H. Chen, T. Wu, Y. L. Xie, Y. J. Yan, R. H. Liu, X. F. Wang, J. J. Ying, X. H. Chen, *J. Phys. Condens. Matter* **2008**, *20*, 422201.
[48] Y. Qi, L. Wang, Z. Gao, D. Wang, X. Zhang, C. Wang, C. Yao, Y. Ma, *New J. Phys.* **2011**, *13*, 033020.

Manuscript received: May 6, 2022
Revised manuscript received: August 25, 2022
Accepted manuscript online: September 4, 2022

